Ocean Systems Engineering, Vol. 1, No. 4 (2011) 337-353
DOI: http://dx.doi.org/10.12989/ose.2011.1.4.337

Numerical analysis of an offshore platform with large partial porous cylindrical members due to wave forces

Min-Su Park*[1], Kenji Kawano[2] and Shuichi Nagata[1]

[1]*Institute of Ocean Energy, Saga University, Saga 840-8502, Japan*
[2]*Department of Ocean and Civil Engineering, Kagoshima University, Kagoshima 890-8580, Japan*
(Received September 14, 2011, Revised December 2, 2011, Accepted December 9, 2011)

Abstract. In the present study, an offshore platform having large partial porous cylindrical members, which are composed of permeable and impermeable cylinders, is suggested. In order to calculate the wave force on large partial porous cylindrical members, the fluid domain is divided into three regions: a single exterior region, N inner regions and N beneath regions, and the scattering wave in each fluid region is expressed by an Eigen-function expansion method. Applying Darcy's law to the porous boundary condition, the effect of porosity is simplified. Wave excitation forces and wave run up on the structures are presented for various wave conditions. For the idealized three-dimensional platform having large partial porous cylindrical members, the dynamic response evaluations of the platform due to wave forces are carried out through the modal analysis. In order to examine the effects of soil-structure interaction, the substructure method is also applied. The displacement and bending stress at the selective nodal points of the structure are computed using various input parameters, such as the shear-wave velocity of soil, the wave height and the wave period. Applying the Monte Carlo Simulation (MCS) method, the reliability evaluations at critical structure members, which contained uncertainties caused by dynamic forces and structural properties, are examined by the reliability index with the results obtained from MCS.

Keywords: large partial porous cylindrical members, eigen-function expansion method, wave excitation forces, substructure method, MCS method.

1. Introduction

An offshore platform with a large deck area is a new concept of offshore structure for utilizing ocean space such as residence areas, airports, and power station, etc. In order to develop a large-scale offshore structure the wave forces on structures and the reaction forces on foundations must be reduced. One possible way is to use a large-diameter partial porous cylindrical member (LPPC member), which is composed of a porous part located near free surface to reduce the horizontal wave force and a rigid part bounded top and bottom by impermeable end caps. It is reported that the porous members can significantly reduce the wave force and wave run up acting on an offshore structure by many researchers (Williams and Li 1998, 2000, Cho and Kim 2010, and Park *et al*. 2010)

In addition, since large platforms have heavy dead loads, the reaction forces on the foundations become severe, thus very firm foundations should be required. Therefore, the dynamic soil-structure

*Corresponding author, Postdoctoral researcher, E-mail: park@ioes.saga-u.ac.jp

interaction has to be fully considered. There are two main methods for the analysis of dynamic structure-foundation interaction, direct and substructure methods, as outlined by Wolf (1985, 1988).

On the other hand, the uncertainty of dynamic forces and structural properties plays an important role on structural reliability. If the uncertainty is limited within small variations, the sensitivity of uncertainties can be effectively evaluated by the perturbation method. When the uncertainty has relatively large variations and the structure motions are nonlinear, the Monte Carlo Simulation (MCS) method would be an effective tool for taking account of the influence of uncertainty (Kawano and Venkataramana 1998, Guan and Melchers 2000 and Park *et al*. 2011). It was also reported that the reliability should be evaluated using the dynamic responses since the effect of uncertainty of dynamic forces is important (Kardeniz 2005).

In the present study, a 3D numerical analysis method is developed with the Eigen-function expansion method and Darcy's law in order to calculate the wave force acting on LPPC members. To deal with hydrodynamic interactions among LPPC members, the fluid domain is divided into three regions: a single exterior region, N inner regions and N beneath regions, and the scattering wave in each fluid region is expressed by the Eigen-function expansion method with using 3-dimension liner potential theory. Applying Darcy's law to the porous boundary, the effect of porosity is simplified. In order to verify the present method, the calculated results are compared with experimental results from Zhao *et al*. (2011) and numerical results of the high-order boundary element method from Choi *et al*. (2000). The wave excitation forces and wave run up on the structures are presented for various wave conditions. By applying the wave force, the dynamic response evaluation of the offshore platform having LPPC members is carried out through the modal analysis with the Newmark method (Park *et al*. 2011) as a time integration scheme. In order to evaluate the effect of soil-structure interaction, the substructure method is also applied to the equation of motion. Therefore, the present three-dimensional platform consists of two subsystems: superstructure and pile-foundation subsystems, which are connected at the nodal points between the pile heads of the foundation and the bottom of the superstructure. Using the reliability index from the MCS method the dynamic response of the platform against uncertain wave forces is fully evaluated. From these results, it is found that this type of offshore structure may be useful to build a large-scale platform by reducing the excitation forces.

2. Formulation

2.1. Wave force evaluation

It is assumed that the computational fluid domain is inviscid, and incompressible, and its motion is irrotational. An arbitrary array of N partial porous cylindrical members is situated in water of uniform depth d and the draughts of each permeable and impermeable cylinder are h and b, respectively. Thus the total draught length of partial porous cylindrical member is $D(= h + b)$. The radius of the jth partial porous cylinder is a_j and the global Cartesian coordinate system(x, y, z) is defined with an origin located on the sea bed with the z-axis directed vertically upwards. The center of each partial porous cylinder at (x_j, y_j) is taken as the origin of a local polar coordinate system (r_j, θ_j), where θ_j is measured counterclockwise from the positive x-axis. The center of the lth partial porous cylinder has polar coordinates (R_{jl}, α_{jl}) relative to the jth partial porous cylinder. The coordinate relationship between the jth and lth partial porous cylinders is shown in Fig. 1.

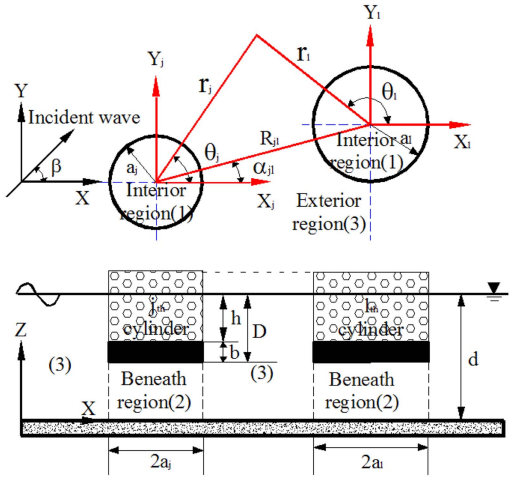

Fig. 1 Coordinate system for an array of partial-porous cylinders

Moreover, the fluid domain is divided into three regions: region 1 above the impermeable cylinder ($r \le a,\ d\text{-}h \le z \le d$), region 2 beneath the impermeable cylinder ($r \le a,\ 0 \le z \le d\text{-}b\text{-}h$), and region 3 which is exterior to the partial porous cylinder and extends to infinity in the horizontal plane ($r \ge a,\ 0 \le z \le d$).

The array of partial porous cylindrical members is subjected to a train of regular waves of height H and angular frequency ω propagating at an angle β to the positive x-axis. When the uniform geometry of the array structure vertically allows the depth dependence in the solution, it can be written as follows

$$\Phi(x,y,z,t) = R_e[-\{igH/(2\omega)\}\phi(x,y,z)e^{-i\omega t}] \tag{1}$$

where, Re[ ] denotes the real part of a complex velocity potential Φ.

The wave potential in the inner region(1) of the jth partial porous cylinder, which satisfies the appropriate free surface and structural boundary conditions, can be expressed by the following Eigen-function expansion

$$\phi_1^j = \sum_{n=-\infty}^{n=\infty}\left[A_n^j J_n(k_0 r_j)\frac{\cosh\{k_0(z-d+h)\}}{\cosh(k_0 h)}\right]e^{in\theta_j} \tag{2}$$

in which J_n denotes the Bessel function of the first kind of order n and A_n^j is the unknown complex potential coefficient. A new wave number k_0 is introduced, which satisfies the dispersion relation $\omega^2 = gk_0\tanh k_0 h$, where g and h denote the gravitational acceleration and local water depth, respectively.

The wave potential in the beneath region (2) of the jth impermeable cylinder, which satisfies the bottom and sea-bed boundary conditions, can be also expressed by the following Eigen-function expansion

$$\phi_2^j = \sum_{n=-\infty}^{n=\infty}\left[\frac{B_{n,0}^j}{2}\left(\frac{r_j}{a_j}\right)^n + \sum_{q=1}^{\infty} B_{n,q}^j \frac{(b_0 r_j)}{I_n(b_0 a_j)}\cos(b_0 z)\right] e^{in\theta_j} \tag{3}$$

in which $b_0 = q\pi/(d\text{-}b\text{-}h)$ and I_n denotes the modified Bessel function of the first kind of order n, respectively. $B^j_{n,0}$ and $B^j_{n,q}$ are the unknown complex potential coefficients.

In addition the wave potential in the exterior region (3), which is expressed by using Graf's addition theorem for the Bessel Functions (Abramowitz and Stegun 1972) and satisfies the Helmholtz equation, can be expressed by the following Eigen-function expansion

$$\phi_3^j(r_j, \theta_j) = \sum_{n=-\infty}^{n=\infty}\left[\begin{array}{c} I_j J_n(kr_j)e^{in(\pi/2-\beta)} + C_n^j Z_n^j H_n^j(kr_j) \\ \sum_{\substack{l=1 \\ l\neq j}}^{N}\sum_{m=-\infty}^{m=\infty} C_m^l Z_m^l H_{m-n}(kR_{lj}) e^{i(m-n)\alpha_{lj}} J_n(kr_j) \end{array}\right] \times e^{in\theta_j}\frac{\cosh kz}{\cosh kd} \tag{4}$$

where $I_j = e^{ik(x_j\cos\beta + y_j\sin\beta)}$ is a phase factor associated with the partial porous cylinder j. k is the incident wave number which is related to the angular frequency through the dispersion relation, $\omega^2 = gk\tanh kd$, with d the water depth. The right-hand side of Eq. (4) represents the incident wave upon the jth cylinder, the scattered wave produced by the jth cylinder, and the re-scattered wave generated by the adjacent cylinders l, respectively. The factors Z_n^j can be determined by the boundary conditions on the partial porous cylinder surface, where for the limiting case of cylinders being rigid leads to

$$Z_n^j (= Z_{-n}^j) = \frac{J_n'(ka_j)}{H_n'(ka_j)} \tag{5}$$

here H_n is the Hankel function of first kind of order n, and J_n' and H_n' are the first derivatives of the Bessel and Hankel function of the first kind, respectively.

In addition to the boundary conditions, each region must be matched to ensure continuity at the interface among regions. Finally, the matching conditions can be written as follows

$$\begin{aligned} &\frac{\partial \phi_1^j}{\partial r} = \frac{\partial \phi_3^j}{\partial r} \qquad on \qquad r_j = a_j,\ d \geq z \geq d-h \\ &\phi_2^j = \phi_3^j \qquad on \qquad r_j = a_j,\ d-h-b \geq z \geq 0 \\ &\frac{\partial \phi_2^j}{\partial r} = \frac{\partial \phi_3^j}{\partial r} \qquad on \qquad r_j = a_j,\ d- \ -b \geq z \geq 0 \end{aligned} \tag{6}$$

As another matching condition, the fluid flow passing through the porous cylindrical surface is assumed to obey Darcy's law. Therefore it can be written as follows (Williams and Li 2000)

$$\frac{\partial \phi_1^j}{\partial r} = \frac{\gamma}{\mu}\rho i\omega[\phi_1^{(j)} - \phi_3^{(j)}] \qquad on \qquad r_j = a_j, \quad j = 1,2,3,\ldots,N \tag{7}$$

where μ is the coefficient of dynamic viscosity, γ is a material constant having the dimension of length and ρ is the fluid density, respectively. Subsequently, the porosity of the cylinder will be characterized by the dimensionless parameter, G. The body boundary condition on the porous cylinder can be expressed with the G.

$$\frac{\partial \phi_1^{\ j}}{\partial r} = ik_0 G[\phi_1^{(j)} - \phi_3^{(j)}] \tag{8}$$

in which, $G = \dfrac{\rho\omega\gamma}{\mu k_0}$

Applying matching conditions in Eqs. (6) and (8), and exploiting the orthogonality of depth, the key equation for unknown coefficients C_n^j can be obtained as follows

$$\begin{aligned} & C_n Z_n^j \left\{ H_n'(ka)kS_6 - \frac{n}{a(d-h-b)} H_n(ka)S_1 - H_n(ka)\frac{S_2}{S_3} - J_n'(k_0a)k_0 H_n(ka)\frac{S_4}{QS_5} \right\} \\ & + \sum_{\substack{l=1 \\ l=j}}^{N} \sum_{m=-M}^{n=M} C_m^l Z_m^l H_{m-n}(kR_{lj}) e^{i(m-n)a_{lj}} \left\{ \begin{matrix} J_n'(ka)kS_6 - \dfrac{n}{a(d-h-b)} J_n(ka)S_1 \\ -J_n(ka)\dfrac{S_2}{S_3} - J_n'(k_0a)k_0 J_n(ka)\dfrac{S_4}{QS_5} \end{matrix} \right\} \\ & = -I_j e^{in(\pi/2-\beta)} \left\{ J_n'(ka)kS_6 - \frac{n}{a(d-h-b)} J_n(ka)S_1 - J_n(ka)\frac{S_2}{S_3} - J_n'(k_0a)k_0 J_n(ka)\frac{S_4}{QS_5} \right\} \end{aligned} \tag{9}$$

where,

$$S_1 = \int_0^{d-h-b} \frac{\cosh kz}{\cosh kd} dz \int_0^{d-h-b} \frac{\cosh kz}{\cosh kd} dz$$

$$S_2 = \int_0^{d-h-b} \frac{\cosh kz}{\cosh kd} \cos(b_0 z) dz \times \int_0^{d-h-b} \frac{\cosh kz}{\cosh kd} \cos(b_0 z) dz \times \sum_{q=1}^{\infty} \frac{I_n'(b_0 z) b_0}{I_n'(b_0 z)}$$

$$S_3 = \int_0^{d-b-h} \{\cos(b_0 z)\}^2 dz$$

$$S_4 = \int_{d-h}^{d} \left\{ \frac{\cosh k_0(z-d+h)}{\cosh k_0 h} \frac{\cosh kz}{\cosh kd} \right\} dz \times \int_{d-h}^{d} \left\{ \frac{\cosh k_0(z-d+h)}{\cosh k_0 h} \frac{\cosh kz}{\cosh kd} \right\} dz$$

$$S_5 = \int_{d-h}^{d} \left\{ \frac{\cosh k_0(z-d+h)}{\cosh k_0 h} \right\}^2 dz$$

$$S_6 = \int_0^{d} \left\{ \frac{\cosh kz}{\cosh kd} \right\}^2 dz$$

$$Q = \left\{ J_n(k_0 a) + \frac{iJ_n'(k_0 a)}{G} \right\}$$

By using a stand matrix technique, the equations on C_n^j can be solved and the unknown coefficients A_n^j, $B_{n,0}^j$ and $B_{n,q}^j$ may then be obtain from Eqs. (8) and (6) by applying C_n^j. In this manner the velocity potential in each fluid region (ϕ_1^j, ϕ_2^j, ϕ_3^j) can be determined.

After solving the velocity potentials, the wave excitation forces on each cylinder are obtained using the integration of pressure on the wetted surface of cylinder. Surge (F_x) and sway (F_y) forces are calculated as follows

$$F_x^i = -i\rho\omega\int_{d-h}^{d}\int_0^{2\pi}\frac{-igH}{2\omega}\{\phi_3^j-\phi_1^j\}a_j\cos\theta d\theta dz \quad \text{on} \quad d-h\le z\le d$$
$$F_y^i = -i\rho\omega\int_{d-h}^{d}\int_0^{2\pi}\frac{-igH}{2\omega}\{\phi_3^j-\phi_1^j\}a_j\sin\theta d\theta dz \quad \text{on} \quad d-h\le z\le d \tag{10}$$

$$F_x^i = -i\rho\omega\int_{d-h-b}^{d-h}\int_0^{2\pi}\frac{-igH}{2\omega}\{\phi_3^j\}a_j\cos\theta d\theta dz \quad \text{on} \quad d-h-b\le z\le d-h$$
$$F_y^i = -i\rho\omega\int_{d-h-b}^{d-h}\int_0^{2\pi}\frac{-igH}{2\omega}\{\phi_3^j\}a_j\sin\theta d\theta dz \quad \text{on} \quad d-h-b\le z\le d-h \tag{11}$$

where Eq. (10) is for porous part and Eq. (11) is for impermeable portion of cylinder.

Heave (F_z) force is also calculated in the same manner by integrating the velocity potential on the cylinder bottom.

$$F_z^i = -i\rho\omega\int_0^{a}\int_0^{2\pi}\frac{-igH}{2\omega}\{\phi_2^j-\phi_1^j\}r_j d\theta dr \quad \text{on} \quad z = d-h-b \tag{12}$$

2.2. The governing equation of motion

In the present study, the dynamic behavior of an idealized three dimensional platform with four large-diameter partial porous cylindrical (LPPC) members as shown in Fig. 2 is evaluated in the time domain. Using the modal analysis with time histories of wave forces the dynamic response of the structure can be obtained.

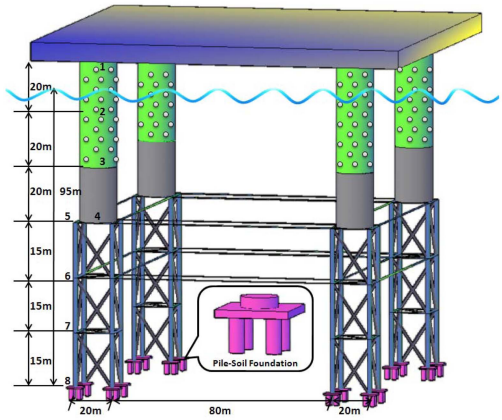

Fig. 2. An idealized three dimensional offshore platform with LPPC members

The platform consists of a framed-structure and a pile-soil foundation subsystem, and has a connection at the base nodal point (node 8) between the pile heads of the foundation and the bottom of the superstructure. Since the two subsystems interact by transferring the displacement and dynamic forces at the pile heads and the truss bases, the governing equation of motion for the entire structure can be formulated as follows

$$\begin{bmatrix}[M_{aa}][M_{ab}]\\ [M_{ba}][M_{bb}]\end{bmatrix}\begin{Bmatrix}\ddot{x}_a\\ \ddot{x}_b\end{Bmatrix}+\begin{bmatrix}[C_{aa}][C_{ab}]\\ [C_{ba}][C_{bb}]\end{bmatrix}\begin{Bmatrix}\dot{x}_a\\ \dot{x}_b\end{Bmatrix}+\begin{bmatrix}[K_{aa}][K_{ab}]\\ [K_{ba}][K_{bb}]\end{bmatrix}\begin{Bmatrix}x_a\\ x_b\end{Bmatrix}=\begin{Bmatrix}\{F_a\}\\ \{F_b\}\end{Bmatrix} \tag{13}$$

where the subscripts 'a' and 'b' denote the unconstrained nodal point on the superstructure and the point connected to the pile-soil foundation system, respectively. $[M]$, $[C]$ and $[K]$ represent the mass matrix, the damping coefficient matrix, and the stiffness matrix of the structure, respectively. The vector $\{F_a\}$ is the external force acting on the superstructure, $\{F_b\}$ is the reaction force caused by the interaction of the structure-foundation system, $\{x_a\}$ is the displacement of the superstructure, and $\{x_b\}$ is the displacement of the base nodal point. The external force on the superstructure can be obtained from the following equation.

$$\{F_a\} = [C_M]\{\ddot{v}_a\}-[C_M]\{\ddot{x}_a\}+[C_a]\{|\dot{v}_a-\dot{x}_a|(\dot{v}_a-\dot{x}_a)\} \tag{14}$$

where,

$$[C_M] = diag[\ \ddots\ \rho\hat{C}_M V\ddots\ ],\ [C_m] = diag[\ \ddots\ \ \rho(\hat{C}_M-1)V\ddots\ ],\ \ [C_D] = diag\left[\ddots\ \ \rho\hat{C}_D\frac{A}{2}\ddots\ \right]$$

$[C_M]$, $[C_m]$ and $[C_D]$ represent the inertia, added mass and drag coefficients matrices, respectively, $\hat{C}_M$ and $\hat{C}_D$ are inertia and drag coefficients, $\ddot{v}_a$ and $\dot{v}_a$ denote the acceleration and velocity of water particles at the unconstrained nodal points, respectively. ρ represents the water density, V is the enclosed volume and A is the projected area in the direction of flow. For convenient and efficient analysis, a linearized drag force obtained by the least square method was applied to the equation of motion. In order to apply the wave force obtained from Eqs. (10) and (11) to the governing equation of motion for the entire structure, it is assumed the horizontal force per unit length may be written equivalently as the inertia part of Morison's equation in Eq. (14) as follows

$$\{F^j_{xandy}\} = [C_M]\{\ddot{v}_{ad}\} = [C_M]\{\ddot{v}_a\} \tag{15}$$

Therefore, the water-particle acceleration $\{\ddot{v}_{ad}\}$ can replace $\{\ddot{v}_a\}$ of Morison's equation in case of partial porous cylindrical members.

Assuming that the relative velocity between the water particles and the structure is a zero mean Gaussian process, the equation of motion (Eq. (13)) can be rearranged as follows

$$\begin{bmatrix}[\tilde{M}_{aa}]\ [M_{ab}]\\ [M_{ba}]\ [M_{bb}]\end{bmatrix}\begin{Bmatrix}\ddot{x}_a\\ \ddot{x}_b\end{Bmatrix}+\begin{bmatrix}[\tilde{C}_{aa}]\ [C_{ab}]\\ [C_{ba}]\ [C_{bb}]\end{bmatrix}\begin{Bmatrix}\dot{x}_a\\ \dot{x}_b\end{Bmatrix}+\begin{bmatrix}[K_{aa}]\ [K_{ab}]\\ [K_{ba}]\ [K_{bb}]\end{bmatrix}\begin{Bmatrix}x_a\\ x_b\end{Bmatrix}=\begin{bmatrix}[C_M]\ [C_D]\\ 0\quad 0\end{bmatrix}\begin{Bmatrix}\ddot{v}_a\\ \dot{v}_b\end{Bmatrix}+\begin{Bmatrix}0\\ \{F_b\}\end{Bmatrix} \tag{16}$$

where, $[\tilde{M}_{aa}] = [M_{aa}] + [C_m]$, $\quad [\tilde{C}_{aa}] = [C_{aa}] + [C_D]$

From Eq. (16), it is expected that the dynamic vibration due to inertia force and the quasi-static displacement caused by the pile-soil foundation system would be located in the superstructure system. They are given by

$$\begin{Bmatrix} \{x_a\} \\ \{x_b\} \end{Bmatrix} = \begin{bmatrix} [I] & [L] \\ 0 & [I] \end{bmatrix} \begin{Bmatrix} \{x_a^c\} \\ \{x_b\} \end{Bmatrix} \tag{17}$$

where, $[L] = -[K_{aa}]^{-1}[K_{ab}]$

x_a^c is the displacement due to the inertia force in the fixed foundation system, and $[I]$ is the unit matrix.

After substituting Eq. (17) into Eq. (16) and multiplying both sides by the transpose matrix of Eq. (17), the equation of motion for the entire system can be rewritten as follows

$$\begin{aligned} &\begin{bmatrix} [\hat{M}_{aa}] & [\hat{M}_{ab}] \\ [\hat{M}_{ba}] & [\hat{M}_{bb}] \end{bmatrix} \begin{Bmatrix} \{\ddot{x}_a^c\} \\ \{\ddot{x}_b\} \end{Bmatrix} + \begin{bmatrix} [\hat{C}_{aa}] & [\hat{C}_{ab}] \\ [\hat{C}_{ba}] & [\hat{C}_{bb}] \end{bmatrix} \begin{Bmatrix} \{\dot{x}_a^c\} \\ \{\dot{x}_b\} \end{Bmatrix} + \begin{bmatrix} [K_{aa}] & [0] \\ [0] & [\hat{K}_{bb}] \end{bmatrix} \begin{Bmatrix} \{x_a^c\} \\ \{x_b\} \end{Bmatrix} \\ &= \begin{bmatrix} [C_M] & [C_D] \\ [L]^T[C_M] & [L]^T[C_D] \end{bmatrix} \begin{Bmatrix} \{\ddot{v}_a\} \\ \{\dot{v}_a\} \end{Bmatrix} + \begin{bmatrix} [I] & 0 \\ [L]^T & [I] \end{bmatrix} \begin{Bmatrix} \{0\} \\ \{F_b\} \end{Bmatrix} \end{aligned} \tag{18}$$

where

$$\begin{aligned} [\hat{M}_{aa}] &= [\tilde{M}_{aa}] \\ [\hat{M}_{ab}] &= [\tilde{M}_{aa}][L] + [M_{ab}] \\ [\hat{M}_{ba}] &= [L]^T[\tilde{M}_{aa}] + [M_{ba}] \\ [\hat{M}_{bb}] &= [L]^T[\tilde{M}_{aa}][L] + [L]^T[M_{ab}] + [M_{ba}][L] + [M_{bb}] \\ [\hat{C}_{aa}] &= [\tilde{C}_{aa}] \\ [\hat{C}_{ab}] &= [\tilde{C}_{aa}][L] + [C_{ab}] \\ [\hat{C}_{ba}] &= [L]^T[\tilde{C}_{aa}] + [C_{ba}] \\ [\hat{C}_{bb}] &= [L]^T[\tilde{C}_{aa}][L] + [L]^T[C_{ab}] + [C_{ba}][L] + [C_{bb}] \\ [\hat{K}_{bb}] &= [L]^T[K_{ab}] + [K_{bb}] \end{aligned}$$

As the structure mass increases, the interaction between the superstructure and foundation system intensifies; thus, the contribution to the dynamic response of the total system increases. An impedance function was used for analysis of the pile-soil foundation system. This function should be calculated within the range of effective frequencies due to the fact that it is generally dependent on the excitation frequency. Impedance coefficients as damping and stiffness matrices were applied to the equation of motion for the foundation system given in Eq. (19) (Yamada *et al*. 1988 and Park

et al. 2011).

$$[M_p]\{\ddot{x}_p\} + [C_p]\{\dot{x}_p\} + [K_p]\{x_p\} = \{R_p\} \tag{19}$$

where the subscript p represents the pile-soil foundation, $\{R_p\}$ is the force from the pile head, and $[M_p]$, $[C_p]$ and $[K_p]$ denote the mass, damping, and stiffness matrix of the foundation, respectively. By combining the force between the superstructure and pile head, the dynamic equilibrium can be obtained as follows

$$[T]^T\{F_b\} = -\{R_p\} \tag{20}$$

Using the substructure method that satisfies the resultant force equilibrium and the compatible displacement at the platform intersection, the equation of motion for the total system, combining Eq. (18) with Eq. (20), is finally formulated as follows

$$\begin{bmatrix} [\hat{M}_{aa}] & [\hat{M}_{ab}] & [T] \\ [T]^T[\hat{M}_{ba}] & [M_p]+[T]^T & [\hat{M}_{bb}][T] \end{bmatrix} \begin{Bmatrix} \{\ddot{x}_a\} \\ \{\{\ddot{x}_p\}\} \end{Bmatrix} + \begin{bmatrix} [\hat{C}_{aa}] & [\hat{C}_{ab}] & [T] \\ [T]^T[\hat{C}_{ba}] & [C_p]+[T]^T & [\hat{C}_{bb}][T] \end{bmatrix} \begin{Bmatrix} \{\dot{x}_a\} \\ \{\{\dot{x}_p\}\} \end{Bmatrix}$$
$$\begin{bmatrix} [K_{aa}] & [0] \\ [0] & [K_p]+[T]^T & [\hat{K}_{bb}][T] \end{bmatrix} \begin{Bmatrix} \{x_a\} \\ \{x_p\} \end{Bmatrix} + \begin{bmatrix} [C_M] & [C_D] \\ [T]^T[L]^T[C_M] & [T]^T[L]^T[C_D] \end{bmatrix} \begin{Bmatrix} \{\ddot{v}_a\} \\ \{\dot{v}_a\} \end{Bmatrix} \tag{21}$$

Given the wave forces, this equation is solved using the modal analysis based on the eigenvalue and eigenvector. Subsequently, the governing equation with a generalized coordinate system $\{y\}$ can be transformed into

$$[I]\{\ddot{y}\} + diag[\ \ddots\ \ 2\tilde{\beta}_j\tilde{\omega}_j\ \ \ddots\ ]\{\dot{y}\} + diag[\ \ddots\ \ \tilde{\omega}_j^{\,2}\ \ \ddots\ ]\{y\} = [\psi]^T[\tilde{P}]_W \tag{22}$$

where $\begin{Bmatrix} \{x_a\} \\ \{x_p\} \end{Bmatrix} = [\Psi]\{y\}$, $\quad [\tilde{P}]_W = \begin{bmatrix} [C_M] & [C_D] \\ [T]^T[L]^T[C_M] & [T]^T[L]^T[C_D] \end{bmatrix} \begin{Bmatrix} \{\ddot{v}_a\} \\ \{\dot{v}_a\} \end{Bmatrix}$

$[\Psi]$ is a modal matrix, $[\tilde{P}]_W$ is wave forces, $\tilde{\omega}_j$ represents the natural frequency at the jth mode for the vibration of the total system, and $\tilde{\beta}_j$ is the corresponding damping ratio including the mechanical, hydrodynamic radiation and the viscous damping. In this study, $\tilde{\beta}_j$ is the Rayleigh type damping and its magnitude is 2% of the jth mode of the superstructure.

2.3. Uncertain parameters and reliability index

The Monte Carlo Simulation (MCS) method can be used in this study to estimate the dynamic response of the platform with the uncertain input parameters. The reliability evaluations for linear response induced by uncertain input can be carried out through the maximum response obtained from the MCS method. In this study, it is assumed that uncertainties can be found in incident wave period, wave height and shear wave velocity of soil. The uncertain parameter (q) is assumed to be a normal distribution and expressed as follows with the mean value $\overline{q}$ and the variation coefficient δ

$$q = \overline{q}(1 + \varepsilon\delta) \tag{23}$$

where ε is a random number with the normal distribution (zero mean and variance=1). Applying these uncertain parameters, the dynamic response can be calculated by Eq. (22). Then, the mean value of the maximum displacement and bending stress can be determined. If the limit state function is given by the most critical case of the dynamic response (e.g., the maximum bending stress), the following reliability index can be described with the results obtained from the MCS method

$$\beta_R = \frac{\overline{R} - \overline{S}}{\sqrt{\sigma_S^2 + \sigma_R^2}} \tag{24}$$

where $\sigma_R = \delta_R \times \overline{R}$

and δ_R denotes the variation coefficient of member strength. Assuming that the mean value $\overline{R}$ and its standard deviation σ_R are independent of time, these values are constant. The stress $\overline{S}$ and its standard deviation are functions of time. The performance of offshore structures based on the limit state function is strongly depended on the reliability index.

3. Numerical and discussion

Fig. 3 shows the comparison between the present numerical results and the experimental data of Zhao *et al*. (2011) for various incident wave frequencies. The computed body is a full-body porous cylinder with an impermeable bottom plate, radius (a) of 0.15 m and draft (h) of 0.3 m. The water depth (d) in the computational domain is 5 m and the incident wave angle (β) is 0^0. The calculated surge and heave forces are normalized by $\rho g(H/2)a^2$. In Fig. 3, based on the relation between the porosity parameter (G) and the opening ratio (τ) in Zhao *et al*. (2011), $G = \frac{(17.8/\varepsilon + 143.2)\tau^2}{2\pi(1 + 1.06\tau)}$, the parameter ($G$) of 1.432 is used for the present comparison, where the opening ratio (τ) is 0.14 and a fixed wave slop (ε) is 0.04633 for the experimental data. It is seen that both numerical and experimental results are well agreed and the surge wave loads on porous body are remarkably

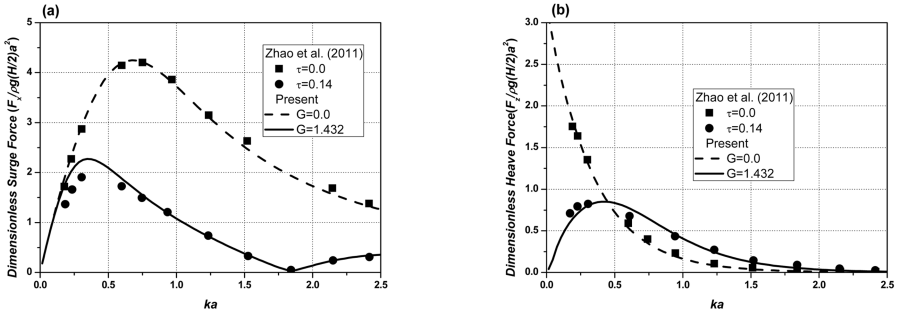

Fig. 3. Comparison of numerical results with experimental results (Zhao *et al*. 2010) for a = 0.15 m, d = 5 m, h = 0.3 m, b =0.0 m, D = 0.3 m and $\beta = 0^0$: (a) Surge force and (b) heave force

smaller than those on impermeable body. It is also observed that the peak frequencies of surge modes for porous body are slightly smaller than the impermeable case, which means the structural property has been changed due to porosity on the cylinder wall. On the other hand, the heave force on the porous body remarkably decreases and goes to zero compared to the impermeable cylinder when ka is less than 0.5, while the force slightly increases with ka greater than 0.5. From this comparison, it is found that in the long waves the heave force is much influenced by the porosity on the side wall. Therefore, this result can be used as an effective means to reduce the heave forces in relatively long waves as installing porous materials on the cylinder wall.

Fig. 4 shows the comparison of total wave forces on four cylinders for various porous wall-lengths (h). The calculation conditions are a = 10.0 m, d = 95.0 m, D = 50.0 m, G = 5.0 and β=0.0^0. The cylinders are numbered clockwise from 1 to 4, and situated at (-50.0, 50.0)m, (50.0, 50.0)m, (50.0, –50.0) m and (–50.0, –50.0) m, respectively. The distance between cylinder centers (R) is 100.0 m, which is 5 times of cylinder diameter (R/(2a) = 5). In the comparison the ratio of h/D = 0.0 and b/D = 1.0 indicates the full-body impermeable cylinder, while h/D=1.0 and b/D=0.0 represents the full-body porous cylinder. In the case of full-body impermeable cylinder, the calculated wave forces are in good agreement with the results from HOBEM (Choi *et al*. 2000). The surge forces of partial-porous cylinders at the modulated peaks gradually decrease as the wave number (ka) increases. The forces at the second and third peaks (at ka = 0.6 and ka = 1.2) decrease about 55.6% and 67.8%, respectively, compared to full-body impermeable cylinder, when the porous-length ratio is only 12.5% of whole draft (h/D = 0.125). However, the reduction rate of surge force is not significant as the ratio increases. It means that the effect of porosity on the body near the free surface is much greater than the case in the deep water. In the comparison of heave forces the partial-porous body has much different from the full-body impermeable case. In particular, in the long wave region, the heave force on the partial-porous body greatly decreases even with a small ratio of porous-length (h/D). The heave forces on porous body are also modulated over a given frequency range, while those on full-body impermeable cylinder decrease monotonously. Through these comparisons, it is found that a cylinder with a small portion of porous-wall near the free surface could be an effective structure to have greatly reduced surge force, and this type of structure can also be useful to control the heave force in the long waves.

Fig. 5 shows the comparison of wave run-up on each cylinder for full-body impermeable and partial-porous cases. The wave run-up is normalized by incident wave height(H) and the abscissa

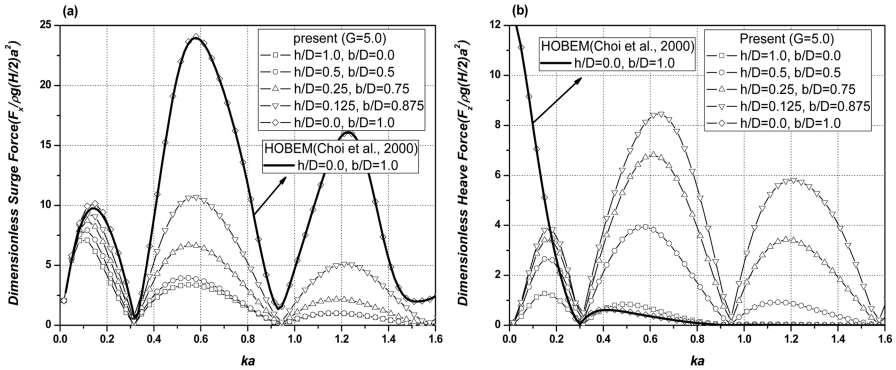

Fig. 4. Comparison of total wave forces on four cylinders with a = 10.0 m, d =95.0 m, R = 100.0 m, D = 50 m, G = 5.0 and β = 0.0^0 for various porosity depths (h): (a) Surge force and (b) heave force

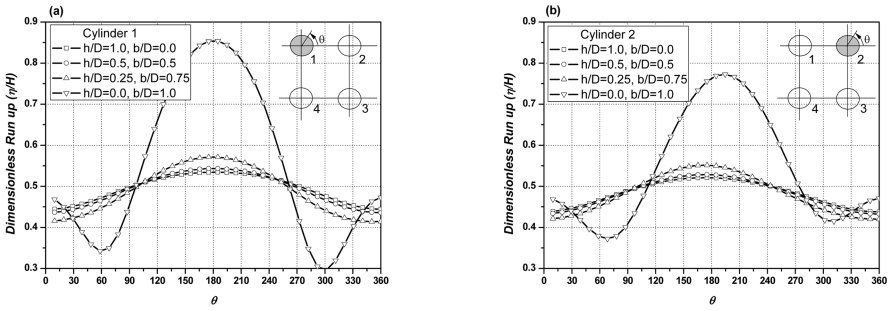

Fig. 5 Comparison of wave run-up on each cylinder for various porosity depths with $\beta = 0.0^0$, $G = 5.0$ and $ka = 0.6$: (a) Cylinder 1 and (b) cylinder 2

denotes the angle(θ) measured counterclockwise from the positive x-axis. Since the hydrodynamic interaction is reduced in the case of porous bodies, the maximum run-up on partial-porous body is significantly lower than the full-body impermeable case. For the cylinder 1 and 2 the maximum values for both surfaced-body conditions are occurred at the similar location, around the angle of 180^0, where the incident wave propagates toward the cylinder. It is found that due to the reduction of wave-body interaction the cases of partial-porous body have similar values regardless of the body locations and the partial-porous body, when the porous-length ratio becomes a larger than 50.0% of whole draft ($h/D = 0.5$), is remarkably effective to reduce the wave run up like the case of full-body porous cylinder.

The dynamic response evaluation of the offshore platform having LPPC members as shown in Fig. 2 is carried out through the modal analysis. In this study the LPPC member, which has a porous-length ratio of greater than 50% (h/D ≥ 0.5), is used based on the above results. These LPPC members can also support the deck weight by excessive buoyancy, thus the resultant reaction forces from base foundation decrease. The height of the platform is 105 m, the width is 120m and the water depth is 95m. The properties of structural materials are unit weight of 77.0 (kN/m^3), Young's modulus of 2.1×10^8 (kN/m^2) and shear stiffness of 8.1×10^7 (kN/m^2). The concentrated load on the deck is assumed to be 4MN on each top point of circular cylinder. Table 1 shows the respective natural periods of the present platform for various soil conditions. Since the pile stiffness increases as the shear-wave velocity of soil increases, the natural period is expected to decrease with the velocity increments (Vs). Therefore, the natural period of the total system is directly dependent on the soil conditions of the foundation. Fig. 6 shows a time histories of displacement at node 1 due to

Table 1. Natural period of offshore platform (sec)

mode	Fixed foundation	Pile-soil foundation (soil condition)		
		$V_s = 100$ m/s	$V_s = 300$m/s	$V_s = 500$ m/s
1st	3.136	3.758	3.336	3.273
2nd	3.097	3.728	3.278	3.214
3rd	3.032	3.650	3.210	3.156
4th	1.737	1.881	1.785	1.775
5th	1.194	1.205	1.200	1.200

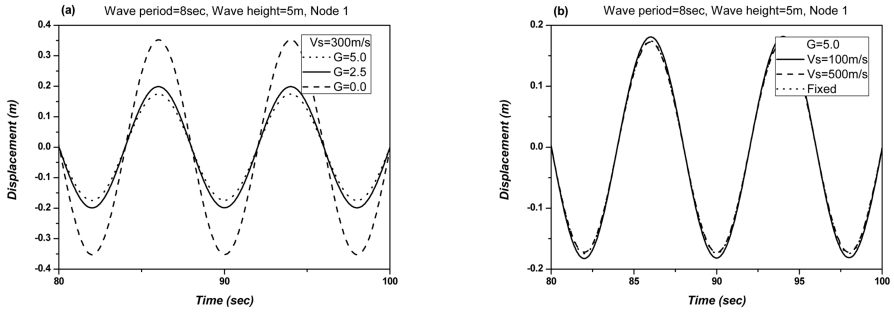

Fig. 6 Time histories of displacement at node 1 due to wave forces with $H = 5$ m and $T = 8$ sec: (a) Vs = 300 m/s and (b) $G = 5.0$

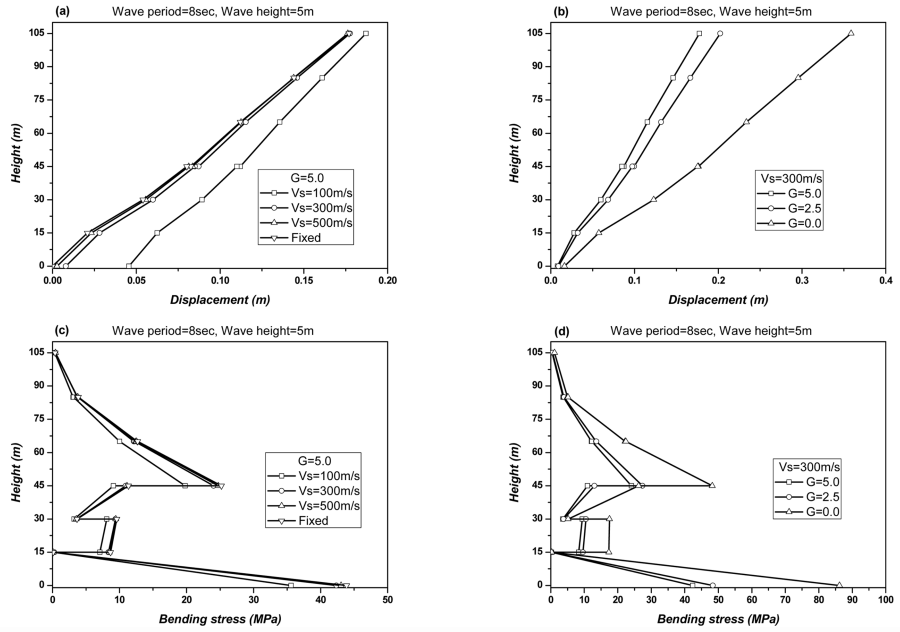

Fig. 7. Comparison of maximum values for all nodal points of rigid structure due to wave force: (a) Displacement for $G = 5.0$, (b) displacement for Vs=300m/s, (c) bending stress for $G = 5.0$ and (d) bending stress for Vs=300 m/s.

wave forces as shown in Fig. 4, where the wave height is 5 m and the wave period is 8sec($ka \approx 0.6$). The phase of displacement for all cases is same regardless of soil condition and porous body surface. In case of porosity ($G = 5.0$), the magnitude decreases 50% compared to the impermeable one. Although the magnitude of displacement of pile-soil foundation system ($Vs = 100$ m/s) is 5% greater than that of fixed case, there is a little difference between fixed and pile-soil foundation with the share wave velocity of 500 m/s. It is understood that the displacement at the top node is strongly influenced by not soil condition but strength of wave forces, and the LPPC member plays an important role on reduction of wave force and displacement of the platform resultantly. Therefore, the LPPC members may be a useful concept for an offshore structure subjected to the severe environmental condition.

Fig. 7 shows the comparison of the maximum values at each nodal point for various shear-wave velocities of soil (*Vs*) and porosity rate (*G*). As the shear-wave velocity decreases (soft soil), the maximum displacement at base nodal point (node 8) greatly increases and the difference between node 1 and node 8 is minimized. These results can be explained by the fact that the incident energy is damped through the pile-soil system and the reaction of the structure becomes small. In the case of the impermeable members ($G = 0.0$), the incident wave energy without loss is acting on the structure and the maximum displacement at the top (node 1) can be expected. Therefore, the greatest difference between $G = 0.0$ and $G = 5.0$ is found at the top deck as shown in Fig (b). The bending stress increases with the velocity increments (firm foundation), and the greatest value is found in a fixed foundation system. As bending stress is generally concentrated at the connection between the different structural systems, the biggest value can be predicted at the bottom of the structure (node 8) where it is connected to the pile-soil foundation, and the second most affected point is observed at the intersection between the LPPC members and the truss structure. Therefore, it is critical for these linked parts to be examined explicitly for the reliable platform design.

In order to evaluate the effects of the wave conditions, the bending stress at node 8 is compared for the various wave periods (Fig. 8). The soil condition with share wave velocity of 300 m/s is chosen for a distinct comparison. As seen in Fig. 8, the case of impermeable members ($G = 0.0$) is significantly influenced by the wave condition since the hydrodynamic interaction is strongly related the wave length, while permeable members ($G = 5.0$) presents considerably constant values. From these results, the offshore structure with LPPC members may be a very useful structure especially in harsh environmental area.

Fig. 9(a) details the convergence of the maximum bending stress at node 8 for the number of simulations (400 times) with variable inputs such as wave period (*T*), height (*H*) and share wave velocity of soil (*Vs*). The variation coefficient (δ) of 0.2 was chosen in the present study. The convergence of all parameters is achieved after 250 simulation numbers. Through this comparison, the effects of the respective uncertain parameters on the dynamic response can be assessed, and reliable results are finally determined after a sufficient number of simulations. The cumulative probability of the bending stress for permeable members with the respective parameters (*Vs, T, H*) is shown in Fig. 9(b). The abscissa denotes the ratio of each maximum response to its mean value, which is determined by a time history of the responses. The wide distribution of the bending stress indicates a significant deviation from the mean value. It is observed that the case of mean wave

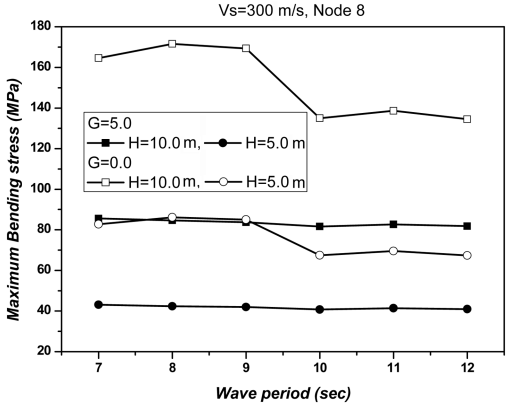

Fig. 8. Maximum bending stress at node 8 due to wave forces

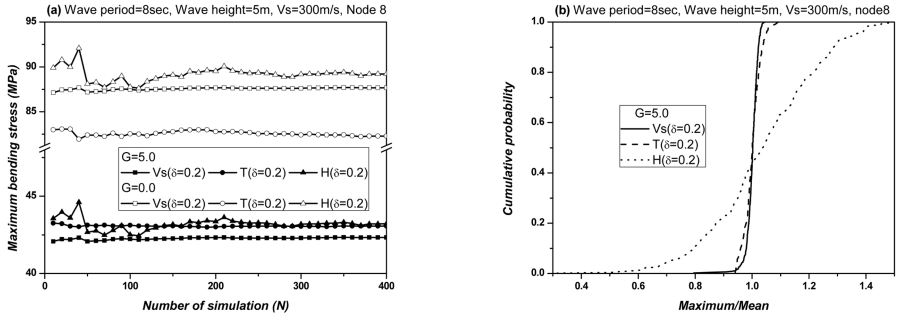

Fig. 9 MCS of the offshore structure with LPPC members at node 8 due to wave forces: (a) Convergence of bending stress and (b) cumulative probability of bending stress

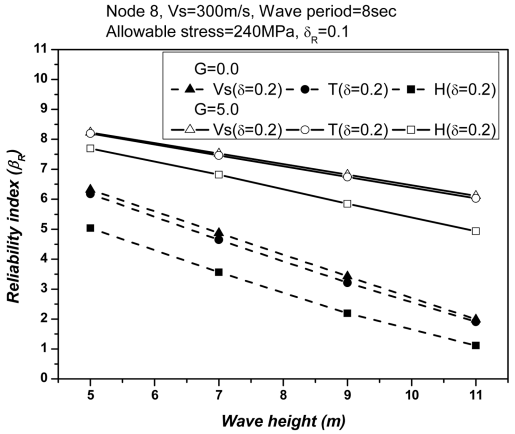

Fig. 10. Comparison of reliability indices at node 8 due to wave forces

height has a broad distribution. As a result, the reliability of the dynamic response is significantly influenced by wave height.

The reliability index expressed with the second moment of the response is suitable for the evaluation of uncertainties. The MCS method is used in order to obtain the second moment, and, subsequently, the reliability of the dynamic responses at critical structure members with respect to uncertain parameters can be evaluated. Assuming that the allowable bending stress is 240 MPa as steel frames and the variation coefficient is 10% (δ_R=0.1), the reliability indices on the bending stress at node 8 for the mean wave height are shown in Fig. 10. The empty and filled symbols represent the cases of permeable and impermeable members, respectively. The reliability index of impermeable members is significantly lower than that with permeable. In general, if the reliability index is greater than three, the structure is considered to be relatively safe. In Fig. 10, the index gradually decreases as the wave height increases. When the height is greater than 9 m, the index of impermeable members is less than three, indicating that the present platform becomes unstable. However, the cases with permeable members are always safe (>3) in the given range of wave height. Through the parametric study, the safety of the platform against the respective uncertain input parameters can be appraised, and the sensitivity of the individual parameters can be determined.

4. Conclusions

The dynamic responses of the bottom-mounted offshore platform with LPPC members due to wave motions are analyzed. In order to calculate the wave force acting on LPPC members the Eigen-function expansion method and Darcy's law is used. By applying the wave force, the dynamic response evaluation of the offshore platform is implemented through the modal analysis with the Newmark method. In addition, the substructure method is applied to the equation of motion in order to evaluate the effect of soil-structure interaction. The results obtained from the present study are summarized as follows:

(1) A LPPC member with small portion of porous-wall near the free surface could be an effective structure to reduce the surge forces and the wave run up as well as to control the heave force in the long waves.

(2) The dynamic response of the platform with porous members is found to be considerably small and be less influenced by the wave condition compared to the case of impermeable members. Thus, the offshore platform with LPPC members may be a useful offshore structure especially in harsh environmental area.

(3) Comparing the fixed foundation system, the pile-soil foundation system has less dynamic responses with given input conditions, so that it can be an efficient way to reduce the response by changing the natural frequency of structure.

(4) By applying the reliability index obtained by the MCS, the present platform was properly evaluated its safety for wave forces. The index values of porous members were larger than those of impermeable members. Therefore, the bottom-mounted offshore platform with LPPC members can be a new promising concept in order to reduce the wave force, wave run up and the resultant dynamic response as well as to ensure the large deck area for utilizing ocean space.

References

Abramowitz, M. and Stegun, I.A. (1972), *Handbook of mathematical functions*, Dover Publications, New York.

Cho, I.H. and Kim, M.H. (2010), "Wave deformation and blocking performance by *N* porous bottom-mounted vertical circular cylinders", *Int. J. Offshore Polar.*, **20**(4), 284-291.

Choi, Y.R., Hong, S.Y. and Choi, H.S. (2000), "An analysis of second-order wave forces on floating bodies by using a higher-order boundary element method", *Ocean Eng.*, **28**(1), 117-138.

Guan, X.L. and Melchers, R.E. (2000), "Acomparison of some FOSM and Monte carlo results", *Applications of Statistics and probability*, ICASP 8, **1**, 65-71.

Karadeniz, H. (2005), "Reliability calculation of RC offshore structures under extreme wave loading", *Proceedings of the 15th Inter. Offshore and polar engineering conference*, ISOPE.

Kawano, K. and Venkataramana, K. (1998), "Dynamic response evaluations of offshore platform with huge deck loads", *Proceedings of the 8th Inter. Offshore and polar engineering conference*, ISOPE.

Park, M.S., Koo, W.C. and Choi, Y.R. (2010), "Hydrodynamic interaction with an array of porous circular cylinders", *Int. J. Nav. Archit. Ocean Eng.*, **2**(3), 146-154.

Park, M.S., Koo, W.C. and Kawano, K. (2011), "Dynamic response analysis of an offshore platform due to seismic motions", *Eng. Struct.*, **33**, 1607-1616.

Williams, A.N. and Li, W. (1998), "Approximate hydro-dynamic analysis of multi-column ocean structures", *Ocean Eng.*, **21**, 519-573.

Williams, A.N. and Li, W. (2000), "Water wave interaction with an array of bottom-mounted surface-piercing porous cylinder", *Ocean Eng.*, **27**(8), 841-866.

Wolf, J.P. (1985), *Dynamic soil structure interaction*, New Jersey: Prentice Hall, Inc., Englewood Cliffs.

Wolf, J.P. (1988), *Soil structure interaction analysis in time domain*, New Jersey: Prentice Hall, Inc., Englewood Cliffs.

Yamada, Y., Kawano, K., Iemura, H. and Venkataramana, K. (1988), "Wave and earthquake response of offshore structure with soil-structure interaction", *Proceedings of the Structure Eng./Earthquake Eng*., JSCE, **5**(2), 361-370.

Zhao, F., Bao, W., Kinoshita, T. and Itakura, H. (2011), "Theoretical and experimental study on a porous cylinder floating in waves", *J. Offshore Mech. Arct*., **133**(1), 301-311.